Aerosol Science and Engineering (2023) 7:474–487
https://doi.org/10.1007/s41810-023-00192-7

ORIGINAL PAPER

Estimation of Particle Emission Rates and Calculation of Human Dose from Arc Welding and Cutting of Stainless Steel in a Simulated Confined Workspace

Norbert Serfozo[1] · **Mihalis Lazaridis**[1]

Received: 26 April 2023 / Revised: 7 July 2023 / Accepted: 12 July 2023 / Published online: 25 July 2023

Abstract
The objective of this study was to estimate the particle emission rates, human dose and retention from two arc welding processes and cutting of stainless steel. The two arc welding processes were Shielded Metal Arc Welding (SMAW) and Tungsten Inert Gas (TIG). In a simulated confined workspace of experimental chamber under controlled conditions, four different scenarios were considered, including the use of filtering face piece respirator (FFR), leaving or staying in the workspace after the emission. Deposited and retained dose in the respiratory tract was assessed for the different regions of the human respiratory tract using a dosimetry model (ExDoM2). The three investigated processes generated high particle number concentrations ranging from 2.4 to 3.6×10^6 particles/cm^3 and were the highest during TIG. Among all three processes, PM_{10} concentrations from cutting reached the highest levels [11 and 22 ($\times 10^3$) μg/m^3], while SMAW had the highest contribution of fine particles [~4.1 ($\times 10^3$) μg/m^3], consisting mostly of $PM_{1–2.5}$. The examination of different scenarios revealed that there is only a slight difference in respect to deposited dose while staying in the workspace for the entire investigated time period (4 h) with or without use of Filtering Facepiece Respirator (FFR). It would be more beneficial in respect to deposited dose if the exposed subject was not wearing a FFR during the emission process and would leave the polluted workspace immediately after the emission period. In the first two scenarios (staying 4 h in the polluted workspace with and without FFR), both welding processes had higher cumulative deposited (~23%) and retained dose (~20%) in thoracic region compared to cutting (~9% and ~7%). These results demonstrate that even a short emission period can cause a considerable increase in concentrations of harmful respirable particles, thus increasing the human dose. The approach applied in this study could be used for the determination of personal exposure and dose to particles of known composition particularly in confined workspaces.

Keywords Arc welding · Stainless steel cutting · Chamber study · Particle emission · Human dose · Cutting of stainless steel · Aerosol emissions · Simulated confined workspace

1 Introduction

Arc welding is a common unit operation in the construction industry, where frequent changes in location and welding position make it more difficult to control fume exposures than in industries where fixed locations are the norm. Shielded Metal Arc Welding (SMAW; also known as Manual Metal Arc Welding—MMAW or 'stick' welding), is a manual arc welding process that uses a consumable electrode of a proper composition for generating arc between itself and the parent work piece. In SMAW, the electrode is a metal rod or stick held in the torch with a small clamp. The rod has a solid coating of inert materials which vaporizes during welding. This creates an inert cloud or gases which protect the molten metal and displace any oxygen that might come into contact with it. The gas cloud settles on the pool of molten metal as it cools, and is referred to as 'slag'. The disadvantage to SMAW is that the slag must be chipped off of the weld after it cools, and can sometimes infiltrate the weld causing weakness. Tungsten Inert Gas (TIG; also known as Gas Tungsten Arc Welding—GTAW), is an arc welding process in which heat is generated by an electric arc struck between a non-consumable tungsten

✉ Mihalis Lazaridis
lazaridi@mred.tuc.gr

[1] School of Chemical and Environmental Engineering, Technical University of Crete, Polytechneioupolis, 73100 Chania, Greece

electrode and the work piece. Flux is not used in the process and the weld pool is shielded by an inert gas (Ar, He, N or as mixture with CO_2) protecting the molten metal from atmospheric contamination. The heat produced by the arc melts the edges of work pieces and joins them, filler rod/wire may be used, if required. Tungsten withstands the heat of welding, significantly less fume is generated in comparison with SMAW, and is usually reserved for specialized types of welds (Antonini 2014).

Welding fumes appear when the arc between a special electrode and a weld material produces evaporation of the welding consumables. The high-temperature multicomponent vapor is forced up from the bottom area of the arc column to the low-temperature environmental air and forms a vapor–gas mixture as a result of mixing with air (Su et al. 2019; Baracchini et al. 2018). The vapor–gas mixture cools down during mixing with air, and reaches a temperature of phase transition, when the primary particles of welding fumes are formed. Their chemical composition and size distribution are of great importance since they determine the physicochemical properties of the welding fume (Berlinger et al. 2011; Oprya et al. 2012; Vishnyakov et al. 2019). The dusty plasma behavior (strong ionization of the environment created by electric-arc discharge formed between the electrode and the weld material) was studied by Vishnyakov et al. (2014a) in the process of coagulation of the primary particles, which are formed as a result of the nucleation and nuclei growth in the condensable high-temperature vapors. The study found that the agglomeration of the ultrafine particles (~2 nm) occurred in two stages. In the first stage the chain-like agglomerates were formed rapidly, and then they associated with the cluster-like agglomerates, and the final agglomerates (inhalable particles) had bimodal size distribution with different chemical compositions and fractal dimensions. The agglomerates are kept together by van der Waals, electrostatic and magnetic forces (Antonini 2006). These agglomerates consist of long chains, frequently of hundreds of fine particles, are rather stable and retain their agglomerate structure in the process of their separation with an electrostatic classifier of SMPS or with a cascade impactor.

Ennan et al. (2013) demonstrated that the inhalable particles of the welding fume have three-modal particle size distribution, when electrodes with rutile (such as the one used in this study) and carbonate-fluorite covers are applied. The first mode (content of 80–90%) is represented by the agglomerates of small primary particles which are formed as a result of nucleation and growth of the nuclei in the liquid phase. The second mode (10–20%) is a product of association of the small primary particles with the large primary particles, which are formed as a result of the coagulation of the nuclei in the liquid phase. The third mode (0.02–0.2%) is the coarse fume particles.

Welding exposure is also a common cause of work-related asthma (WRA), which includes both occupational asthma (OA, new-onset asthma related to sensitizers or irritant work exposures) and work-exacerbated asthma (WEA, pre-existing asthma that worsens on work exposures). Banga et al. (2011) found that exposure to welding fumes was the fifth leading cause of WRA among workers in Michigan, US. Antonini et al. (2011) reported respiratory effects among welders including bronchitis, airway irritation, lung function changes, and a possible increase in the incidence of lung cancer. Welders may be exposed to ultrafine particles (UFP; $\leq$100 nm) (Debia et al. 2014; Graczyk et al. 2015; Ward et al. 2020) and a variety of toxic airborne contaminants including manganese (Mn) and hexavalent chromium (Cr^{VI}) (Hobson et al. 2011). This issue of occupational UFP exposures is of increasing importance as evidence suggests that UFPs are potent triggers of oxidative stress, systemic inflammatory and may contribute to adverse respiratory outcomes as specific exposure to welding fumes is known to cause respiratory health problems (Järvelä et al. 2013; Kauppi et al. 2015).

General ventilation systems, consisting of both supply and exhaust, mechanical, natural, or a mixture of both might prevent or minimize the respiratory hazards of welding fume. The most efficient and economical method of welding contaminant control in the breathing zone of the welder is local exhaust that captures the contaminants at or near the source (Flynn and Susi 2012). When ventilation controls fail to reduce the air contaminants produced by welding to allowable levels (Pouzou et al. 2015) or when the use of ventilation is not feasible (e.g., welding in confined spaces), personal respiratory protective equipment, such as filtering facepiece respirator (FFR) should be used for protection (Lehnert et al. 2012) from exposure to hazardous levels of airborne contaminants of full-time welders (boilermakers, pipefitters, construction workers, shipbuilders, automotive workers). When welding in a confined space (area with poor ventilation that has limited space, entry or exit, such as storage tanks, holds of ships, boilers, furnaces, tunnels), all the hazards that are associated with normal welding are amplified (Bowler et al. 2007).

However, up to this day, there is just a limited research on emission rates and resulting exposure dose from welding in confined workspaces in regards to both, field and simulated studies. Hazardous gases and fumes may accumulate rapidly, thus causing a reduction in safe, breathable air (Hanley et al. 2015; Paridokht et al. 2023). Computational fluid dynamics (CFD) was used by Tian et al. (2016) to investigate the transport and deposition of welding fume agglomerates in a realistic human nasal airway and found that a very small fraction of the inhaled welding fume agglomerates is dispersed into the nasal olfactory mucosa, and did not reach the olfactory bulb within the brain. The majority of particles

passed through the nasal barrier and penetrated deep into the lungs.

The aim of the current study was to estimate the emission rates, and human dose and retention from two arc welding processes, SMAW and TIG. Additionally, cutting of stainless steel (SS) was also investigated as this process many times accompanying the welding (Serfozo 2017). In a simulated confined workspace of experimental chamber under controlled conditions, 4 different exposure scenarios were considered, including the use of FFR, leaving the workspace or staying in the workspace after the emission. In this study, total deposited dose in the Respiratory Tract (RT) was assessed for the extrathoracic and the thoracic region of the human respiratory tract, subsequently, cumulative retention in extrathoracic and thoracic regions, Gastrointestinal (GI) tract and blood was also calculated. Dose and retention from SMAW, TIG and cutting of SS were calculated for exposure period of 4 h under 4 different scenarios where the emission period occurred in the first 5 min.

2 Experimental

2.1 Materials and Methods

Measurements were conducted in a small stainless steel environmental chamber with volume of 7.56 m^3 (Serfozo et al. 2018). The flow through the chamber was 5.3 LPM measured with Gilibrator-2 (Standard cell, Sensidyne, USA), thus, the air exchange rate (AER) was equal to 0.044 h^{-1}. Additional pump to increase the Air Exchange Rate (AER) was intentionally not employed to simulate confined welding workspace. Its interior dimensions are $2.50 \times 2.39 \times 1.27$ m^3 (H × L × W), built from double-layered drywall (75 mm) with aluminum skeleton and interior surface covered with 1.5 mm thick Stainless Steel (SS) sheets. Outdoor air entering the chamber is purged through HEPA filter (type H14; 610 mm × 305 mm × 69 mm; 99.995% removal efficiency). Chamber features fixed window (510 × 410 mm), door (2110 × 805 mm), two openings for inlet/outlet, and a sealed tube opening for a glove (PVC Gauntlet) designed to enable operating inside the chamber without entering it. The inlet of the sampling point was in distance of 1.2 m from the emission source. Chamber and the sampling tubes were tested for leaks prior to the beginning of the measurements and the particle number and mass concentration were monitored continuously. Uniform particle concentration was ensured by fan operating at 1200 rpm. The air temperature and relative humidity inside the chamber during all the measurements was on average 25 ± 1 °C and 45 ± 1%, respectively. Metal used to weld and cut in all experiments was stainless steel tube (100–150 mm) with rectangular profile and wall thickness of 2.5 mm.

SMAW was performed by Gysmi 164 Inverter (Gys, France) with Fincord-M (350 mm, Ø = 4 mm) rutile medium coated electrodes (Oerlikon, Switzerland) at 90 A of direct current (DC), which was sufficient enough considering the SS tube wall thickness. In total, one electrode was used for both SMAW welding processes (1/2 electrode per process). In this study, TIG welding by fusion (i.e., without a filler rod) was performed by Fronius Magic Wave 2000 (Fronius, Austria) with argon (100% Ar) as an inert gas at DC of 90 A. For the cutting experiments AG 115 SS-DC angle cutter (Kraft Tech, China) equipped with Speed Plus 200 Green cutting disc for stainless steel (Zebra, Würth, Germany) was employed to cut the SS tube. The net duration of the emission source was approximately 3 × 20 s and 2 × 60 s (total time period of 5 min per experiment) for welding processes and cutting, respectively. These relatively short emission periods are based on limitations of the used instrumentation where after certain concentration limit flow rate and coincidence error occurs. Each experiment was done two times in a row for each process on a same day with a minimum of 4–6 h between the processes, and measurements of different processes were conducted on different days. The effect of different current, welded metal, welding duration, distance of sampling point or AER was not examined (Serfozo et al. 2017a).

2.2 Instrumentation

Condensation Particle Counter (CPC 3775) was employed to measure the total particle number concentration, an OPS to measure the mass concentrations of different particles sizes (both TSI, Inc., USA) and a PhoCheck instrument (ION Science) for the estimation of the total volatile organic compound (TVOC). CPC 3775 samples particles up to 3 µm for concentrations up to 5×10^4 particles /cm^3 with continuous, live-time coincidence correction in single particle counting mode and from 5×10^4 to 10^7 particles /cm^3 in photometric mode, and was sampling in high-flow mode at 1.5 LPM flow rate. The OPS is based on 120 light scatter and filter sampling and it is able to count mass concentrations in the range 0.001–275,000 µg/m^3 and number particle concentrations up to 3000 particles /cm^3 in the size range 0.3–10 µm. It operates with up to 16 user-adjustable channels at a sample air flow rate and sheath air flow rates of 1.0 LPM. The mass size distribution data were obtained from the OPS (3330, TSI). Number size distribution data were converted automatically to mass size distribution using the algorithm of the instrument. The total volatile organic compound was measured with a PhoCheck Tiger (ION Science) which uses a photoionisation detection (PID) having a resolution from 1 ppb to 20,000 ppm (calibrated to isobutylene at 20 ℃ at RH equal to 90% with concentration up to 3000 ppm) at flow rate of 0.3 LPM.

In addition, average of total losses due to diffusion, inertial deposition and gravitational settling in the sampling tubing (Hinds 1999) in the chamber measurements for the particle size range found in this study were negligible for CPC as they were estimated to be less than 4% for the particle size range detectable by the instrument. Although the average loss for fine mode particulate mass measured by OPS was also less than 4%, for the coarse mode it was 56% on average, thus loss correction factor was applied for each of the 16 size bins separately for the whole size range measured by the instrument (Serfozo 2017a).

2.3 Deposition Losses Calculation

While in this study the air exchange rate is a known parameter (0.044 h^{-1}), analyses needed to be performed also on overall particle loss rate from the particle number and mass concentration decays to estimate the loss rate β (h^{-1}) comprising all deposition mechanisms. Overall particle loss rate (λ^*) includes the deposition rate of aerosol particles (β) and air change rate (λ):

$$\lambda^* = \lambda + \beta \tag{1}$$

The overall particle loss rate can be derived from a simple mass balance equation (Smolík et al. 2005) describing the change in concentration of aerosol particles in an indoor environment:

$$V\frac{dC_i}{dt} = V\lambda\left(PC_o - C_i\right) + Q - S \tag{2}$$

where V is the volume of the room, C_i and C_o are the concentrations of aerosol particles indoors and outdoors, t is time, λ is the air exchange rate, P is the penetration factor, Q represents possible particles sources and parameter S represents total sink strength of aerosol particles. Assuming that there are no indoor particle sources, that particles are not resuspended, are physically and chemically stable, and there is no coagulation, the sink strength S can be simplified to $S = C_i V \beta$, where β is the deposition rate in the room comprising all deposition mechanisms and all surfaces. Equation (2) can be simplified under the following conditions: (1) after the emission period there is no other source of aerosol particles in the room; (2) there is no resuspension of deposited aerosol particles; (3) particle coagulation can be neglected, (4) the initial aerosol particles concentration C_i is equal to the initial condition $C_i(0) = C_0$. Then the analytical solution of the Eq. (2) describing the loss of aerosol particles becomes:

$$C_i(t) = C_\infty + \left(C_0 - C_\infty\right)e^{-\lambda^* t} \tag{3}$$

The term C_∞ is a function of the initial concentration, volume of the microenvironment (chamber), emission and infiltration rates. The experimental curves were then fitted with the model utilizing the constrained Nelder-Mead Simplex method to find parameters of the model equation which minimize the sum of squares of residuals between theoretical prediction and experimental data.

2.4 Dosimetry Model

The ExDoM2 model was used for the calculations of human dose, which is a dosimetry model for calculating the human exposure and the deposition, dose, clearance, and finally retention of aerosol particles in the respiratory tract (RT) at specific time intervals during and after exposure, under variable exposure conditions (Chalvatzaki and Lazaridis 2015; Chalvatzaki et al. 2020, 2022). The ExDoM2 is an updated version in respect to the ExDoM (Aleksandropoulou and Lazaridis 2013) incorporating modified particle clearance mechanisms in the Human Respiratory Tract Model of International Commission on Radiological Protection (HRTM, ICRP 2015) and it was developed using the Matlab software (Mathworks, Inc., USA) in the Laboratory of Atmospheric Aerosol at the Technical University of Crete. The RT is treated as two regions: the extrathoracic regions (ET) and the thoracic regions (TH). The extrathoracic regions are further divided into the ET1 (anterior nasal passage) and ET2 (posterior nasal passages, pharynx and larynx) regions. The thoracic region (the lungs) is divided into the BB (trachea and bronchi), bb (bronchiolar) and AI (alveolar–interstitial).

The ExDoM2 model estimates the individual's dose rate H (μg/h) of particles in different size fractions by Eq. (4) as the product of the exposure concentration, the ventilation rate and the deposition fraction of particles in the respiratory tract (Chalvatzaki and Lazaridis 2015):

$$H = \sum BC_i n_{i,j} \tag{4}$$

where B (m^3/h) is the ventilation rate of the exposed individual (depending on the breathing frequency and tidal volume), C_i the exposure concentration (μg/m^3) for particles in the size fraction i, and $n_{i,j}$ the deposition fraction in region j of the respiratory tract for particles in the size fraction i. The deposition efficiency n_j depends on aerodynamic deposition efficiency n_{ae} (due to impaction and gravitational settling) and thermodynamic deposition efficiency n_{th} (due to diffusion). The deposition efficiency of region j is calculated as:

$$n_j = \left(n_{ae}^2 + n_{th}^2\right)^{1/2} \tag{5}$$

where both the aerodynamic and thermodynamic efficiencies are expressed as:

$$n = 1 - \exp(-aR^p) \tag{6}$$

where a and p are dimensionless constants and R has a characteristic functional form that is different in each region and

depends on the particle size (aerodynamic and thermodynamic) and the relevant respiration parameters.

The model also calculates the clearance and retention of particles in the RT. The amount of particles in each region of the lungs after an acute intake is given by the mass balance equation (Aleksandropoulou and Lazaridis 2013):

$$\frac{dR_i(t)}{dt} = -\left[m_i(t) + s_i(t)\right]R_i(t) \tag{7}$$

where, $m_i(t)$ and $s_i(t)$ are the instantaneous clearance rates of the deposit in compartment i due to mechanical movement and absorption into blood, respectively, and $R_i(t)$ the retained mass after time t.

The mass of particles retained in the human body includes the deposited mass in each compartment of the RT during and after continuous exposure to particles and their fraction transferred to the GI tract, lymph nodes, and blood. The retained mass in each compartment of the RT and their mass fraction transferred to the oesophagus and blood is estimated by Eq. (8) for fraction of particles dissolving relatively rapidly and Eq. (9) for fraction of particles dissolving slowly, and are solved independently using exponential substitution and Gauss elimination (Chalvatzaki and Lazaridis 2015):

$$\frac{dI_j(t)}{dt} = \sum_{k=1}^{13}\left[m_{k,j}I_k(t) + \left(m_{j,k} + s_r\right)I_j(t)\right] + f_r H_j(t) \tag{8}$$

$$\frac{dT_j(t)}{dt} = \sum_{k=1}^{13}\left[m_{k,j}T_k(t) + \left(m_{j,k} + s_s\right)T_j(t)\right] + \left(1 - f_r\right)H_j(t) \tag{9}$$

where m is the mechanical movement rate of particles from compartment k to j ($m_{k,j}$) or the opposite ($m_{j,k}$), f_r the fraction dissolved rapidly, $(1-f_r)$ the fraction dissolved slowly, s_r the rapid dissolution rate, s_s the slow dissolution rate, H_j the instantaneous dose applied to the compartment j at time t, I the retained mass of particles dissolving relatively rapidly after time t in compartments k and j, T the retained mass of particles dissolving slowly after time t in compartments k and j. Hence, the retained mass after time t in compartment j is calculated as the sum of the $T_j(t)$ and $I_j(t)$. The fractions f_r and $(1-f_r)$ depend on the type of the absorption behavior. The system is solved per 1/(breathing frequency) during exposure and per minute post-exposure to determine retention. For more details about the exposure model see Aleksandropoulou and Lazaridis (2013), and Chalvatzaki and Lazaridis (2015).

Conversion from optical to aerodynamic diameter (Hinds 1999) was needed prior to calculation of exposure dose. For this purpose, uniform value of particle density equal to 3.7 g/cm^3 (Avino et al. 2015) was considered for all the emission sources (SMAW, TIG and cutting). Exposure dose rates from concentration (Base line concentration, BC) in the laboratory (considered as 'clean environment' for the purposes of this study) were taken as the reference and compared to the exposure dose from welding and cutting. Particle density of 1.5 g/cm^3 (approximation for ambient aerosol) was used for the exposure dose calculation of the BC. In all calculations (diameter conversion, BC and exposure dose from emissions), particles were assumed to be spherical (shape factor of 1). Scenarios involving use of FFR in this study were based on FFR filter efficiency of 3 M 8835 from FFP3 filtering class (Serfozo et al. 2017a, b) only in model calculations (FFR was not challenged with welding fumes). The dose rates were calculated for an adult Caucasian male with ventilation rate 1.5 m^3/h (light work scenario, nose breathing, moderate blood absorption behavior) for total of 4 h exposure duration in 1 h exposure time steps for 4 different scenarios where the emission (welding or cutting) occurred in the first 5 min:

Scenario 1: Stay all the time period (4 h) in the polluted workspace without a use of FFR.

Scenario 2: Stay all the time period (4 h) in the polluted workspace; use of FFR only during the emission period (first 5 min).

Scenario 3: Stay in the polluted workspace only for the time period of emission (first 5 min) without a use of FFR and then leave the polluted workspace (to clean environment).

Scenario 4: Stay all the time period (4 h) in the polluted workspace; use of FFR for the entire period.

3 Results and Discussion

3.1 Effect of Welding and Cutting on Particle Number Concentration

During welding and cutting processes the total particle number concentration (TPNC) reached its peak within 5 min from the start of the emission and ranged from 2.4 to 3.6×10^6 particles/cm^3 (see Fig. 1). The 1 h average TPNC varied from 2.4 to 5.2×10^5 particles /cm^3 and was the highest in the case of SMAW and the lowest in the case of cutting process (Table 1). It was not possible to measure the size distributions of the particles emitted during the processes due to technical error of the SMPS and the only available particle size distribution is from SMAW testing on SS at 70 A in a size range of 5–350 nm (see Fig. 2). Note that all the experiments were conducted with DC of 90 A, thus, the concentration would reach higher number concentrations since the emission of airborne fine particles and fume formation rate increases with the current intensity (Guerreiro et al. 2014). As it can be seen in Fig. 2, there is a burst of new particles in the whole measured size range at the start

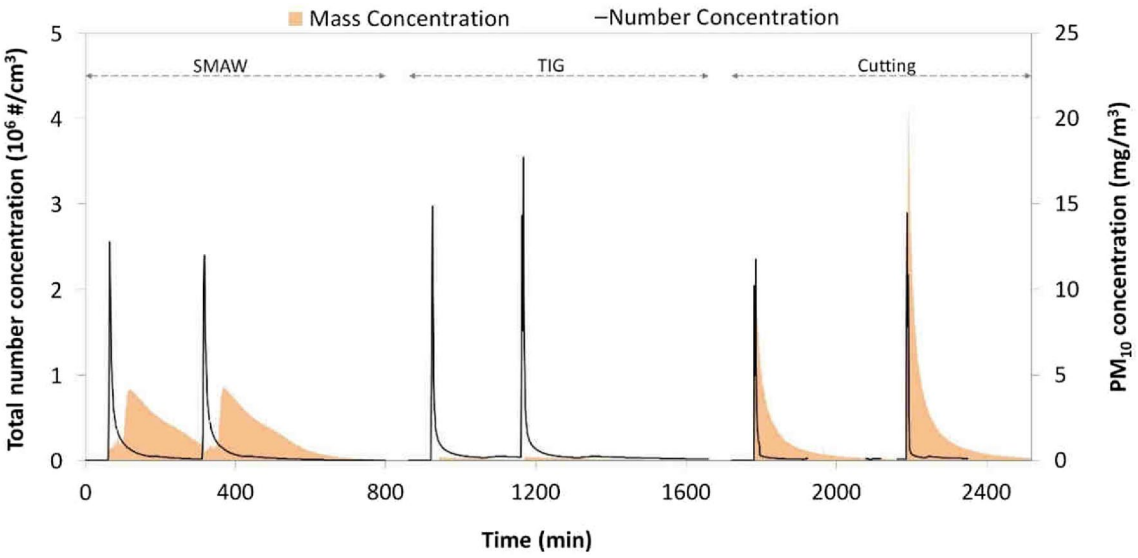

Fig. 1 Total particle number and PM_{10} concentration during welding (SMAW, TIG) and cutting of SS. A CPC 3775 was used to measure the total particle number concentration and an OPS to measure the PM_{10} mass concentrations

Table 1 Average, maximum and minimum number and mass concentration values for period of from the start of welding (SMAW and TIG) and cutting of SS processes

Process	Number concentration (particles/cm^3)			Mass concentration [($\times 10^3$) μg/m^3)]					
				Fine ($PM_{2.5}$)			Coarse ($PM_{2.5-10}$)		
	Aver.	Max.	Min.	Aver.	Max.	Min.	Aver.	Max.	Min.
SMAW I	5.1×10^5	2.6×10^6	3.5×10^4	1.56	4.08	0.09	0.07	0.12	0.03
SMAW II	5.2×10^5	2.4×10^6	1.3×10^5	1.46	4.19	0.32	0.05	0.09	0.03
TIG I	3.9×10^5	3.0×10^6	8.1×10^4	0.18	0.21	0.16	0.01	0.01	0.00
TIG II	4.8×10^5	3.6×10^6	8.7×10^4	0.19	0.21	0.18	0.01	0.01	0.00
Cutting I	2.4×10^5	2.4×10^6	7.1×10^3	1.03	1.64	0.19	3.35	9.41	1.16
Cutting II	2.9×10^5	2.9×10^6	3.1×10^4	1.63	2.64	0.18	6.06	19.28	1.75

of the emission with dominant mode on 13 nm (Fig. 2a). Within 10 min the size distribution shifts towards particles with bigger diameters and higher concentration with dominant mode on 242 nm and reaches its maximum after 15 min from the beginning of the emission. Even 4 h after the end of emission, the size distributions remained almost unchanged, but the particle concentration decreased with time (Fig. 2b). Berlinger et al. (2011) showed that in TIG welding, most particles have mobility diameters 15–160 nm, while SMAW particle diameters are larger, ranging between 100 and 600 nm.

Multicomponent condensation in the low-temperature plasma, which forms at SMAW, was investigated by Vishnyakov et al. (2014b). The liquid particles after nucleation of the predominant component (iron) had bimodal size distribution with a nano-sized mode of nuclei and a larger-sized mode of the aggregated droplets. Consequently, the condensation of the accompanying low-volatility components on these droplets caused the termination of nucleation earlier. Therefore, the growth of the nuclei subsequently occurred by particle coalescence (large number density of nuclei in a liquid state causes their intensive Brownian coagulation). Thus, size distributions in the beginning of the welding process are undergoing rapid changes, hence, SMPS with low-time resolution is not sufficient and a spectrometer, such as Fast Mobility Particles Sizer (FMPS) with time resolution of 1 s might be required (Brand et al. 2013; Avino et al. 2015).

3.2 Effect of Welding and Cutting processes on Particulate Mass Concentration

The 1 h average PM_{10} concentrations during cutting were the highest among all processes (Fig. 1) and reached their maximum [11 and 22 ($\times 10^3$) μg/m^3 for the first and second experiment, respectively] within 5 min from the start of the emission, similarly, as it was in the case of TIG, which had the lowest PM concentrations. Note that due to OPS's coincidence error (when the particle concentration reaches

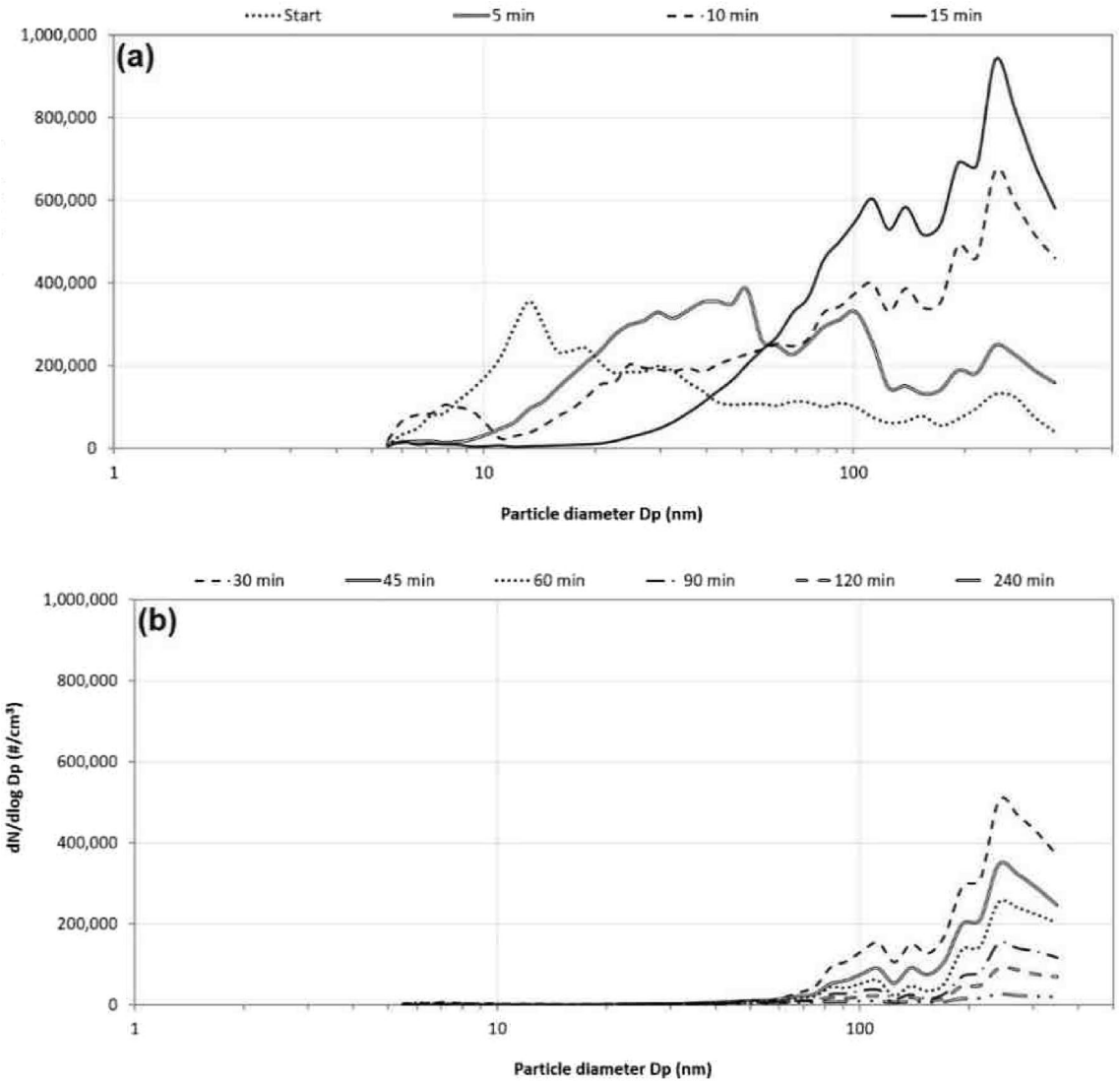

Fig. 2 Size distributions of 5–350 nm particles during SS SMAW test at 70 A using an OPS instrument at different size fractions

the limit of 3×10^3 particles/cm^3), the instrument stopped sampling for about 10 min from the start of the emission in both cases, so the maximum mass concentration would be approximately 0.02 ($\times 10^3$) μg/m^3 higher. As shown in Table 1, fine particles ($PM_{2.5}$) dominated in both welding processes, whereas coarse particles in the cutting process. Mass concentration values during SMAW and cutting processes found in this study are consistent with a study of Lin et al. (2014), where the authors characterized aerosol particle sizes in workplace of fitness equipment manufacturing. The PM_{10} concentration from the SMAW process reached maximum peak [4.14 ($\times 10^3$) μg/m^3 on average] 1 h after the start of emission in both cases, with 1 h average PM_{10} concentration equal to 1.55 ($\times 10^3$) μg/m^3.

Figure 3 illustrates the forming of the three fractions of agglomerates in the welding fume from SMAW consisting mostly of particles in the $PM_{1\text{-}2.5}$ fraction. As mentioned earlier, when the high-temperature multicomponent vapor is transported from the bottom area of the arc column to the low-temperature environmental air, it forms a vapor–gas mixture and reaches a temperature of phase transition when the large primary particles of welding fumes are formed, and at the same time, the mass of the small primary particles decrease. The PM_1 fraction represents the small primary particles' agglomeration fraction, whereas the $PM_{1\text{–}2.5}$ fraction refers to particle structures with a uniform dense core, which are formed as a result of particle coagulation of small and large primary particles. Finally, the $PM_{2.5\text{–}10}$ fraction consists of coarse fume particles (Berlinger et al. 2011; Ennan et al. 2013; Vishnyakov et al. 2014a).

Although in this study the aerosol concentration in the chamber was assumed to be uniform, the distance of the

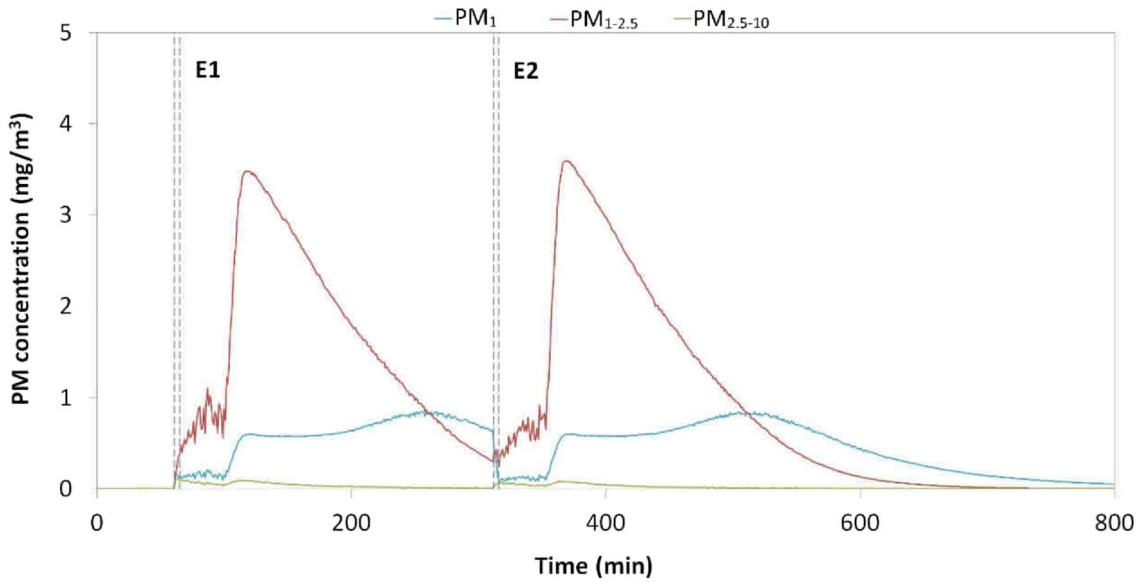

Fig. 3 Concentration of PM_1, $PM_{1–2.5}$ and $PM_{2.5–10}$ during SMAW. E1 and E2 represents the first and the second emission period, respectively

Table 2 Deposition loss rate β (h^{-1}) calculated from particle number and mass concentration decays after the end of emission in a simulated confined workspace

Process	Number concentration (≤ 3 µm)	Mass concentration	
		Fine ($PM_{2.5}$)	Coarse ($PM_{2.5–10}$)
SMAW II	1.334	0.445	1.030
TIG II	3.274	0.247	1.844
Cutting II	1.337	1.093	3.480

Table 3 TVOC concentrations (ppm) in the chamber for period of 12 h

Process	Average	St. deviation	Maximum	Minimum
SMAW II	3.21	0.32	23.17	2.91
TIG II	2.31	0.41	6.86	1.89
Cutting II	0.03	0.03	0.08	0.00

sampling point from the emission source was 1.2 m. Distances 2–5 m from the emission source are sufficient to describe the general background of air pollution in a workroom, but are deficient for determination of personal exposure. The distance of sampling point should be in the radius of ~ 300 mm from the welder's head (Hariri et al. 2013), preferably sampled by personal sampling method (Quémerais et al. 2015) so that solution with fixed sampling position is avoided.

3.3 Deposition Loss Rate

The deposition loss rate was calculated from the particle mass and number concentration decay after the end of particle emission (see Table 2) shows that particulate mass from cutting process had the lowest deposition loss rate for both, fine and coarse mode. On the other hand, particles emitted from SMAW process, despite of high number and mass concentrations, were deposited faster due to the highest particulate mass among all 3 studied processes. Although there were very low concentrations of coarse particles during the welding processes, generally, coarse particles in all 3 cases had lower deposition loss rates than fine particles. Particulate mass generated from TIG welding process had the highest deposition loss rate (not taking into account coarse particles due to its very low contribution to PM_{10}) and the lowest deposition loss rate calculated from number concentration decay suggesting that these particles were smaller in diameter and had lower mass than the particles generated from SMAW or cutting. Number concentration 16 h after the end of TIG emission was still 3.4×10^3 particles/cm^3, while the number concentration for particles generated from SMAW dropped below 2×10^3 particles/cm^3 8 h after the end of emission and decreased to 60 particles /cm^3 after 16 h.

3.4 Effect of Welding and Cutting on TVOC concentrations

As can be seen in Table 3, SMAW produced higher average total volatile organic compound (TVOC) and also had the highest maximum concentration. Average TVOC concentrations were found to be 3.21 and 2.31 ppm for SMAW

and TIG, respectively, and were higher than the average TVOC during cutting of SS (0.03 ppm). This difference can be attributed to the different nature of the welding and cutting processes. The iron oxide particles generated during the process of friction of cutting disc and the SS do not produce high TVOC, whereas in the welding process, much higher temperatures at the melting of electrode and metal produce higher TVOC values. Berlinger et al. (2011) examined the physicochemical characteristics of different welding aerosols and found clear size dependency of the elemental composition in particles generated in SMAW welding. Small particles with diameters below ~ 50 nm are mostly metal oxides, in contrast to larger particles which also contain more volatile elements such as Na, K, S and F, and the amounts of the more volatile elements in the particles seemed to increase with increasing particle size, which explains higher TVOC during SMAW in comparison with cutting.

3.5 Particle Dose in the Human Respiratory Tract

The first exposure scenario, staying in the polluted workspace for the entire time period without a use of FFR, was the 'worst-case' scenario and reached the highest values of deposited, and thus retained dose during all processes (Table 4 and Fig. 4a). Nonetheless, in the second scenario, when the exposure subject is staying in the workspace for the entire time period and FFR is used only for the duration of the emission period (5 min) and then is taken off, deposited dose was lower, but similar to the first scenario (especially in the thoracic region), giving 174-fold, 123-fold and fivefold increase in total deposited dose compared to BC (76 µg) for cutting, SMAW and TIG, respectively. In the third scenario, as demonstrated in Fig. 4b, it would be more beneficial in respect to deposited dose if the exposed subject not wearing a FFR at the duration of emission, would leave the polluted workspace immediately after the emission period (5 min). In such a case, the increase in total deposited dose was estimated to be 19-fold, onefold and 0.3-fold for cutting, SMAW and TIG, respectively, in comparison to the dose from BC. Note that in the case of SMAW in the third scenario, compared to the previous two scenarios, the deposited dose decreased significantly because the average PM_{10} concentration during the emission period (when the subject was still present in the polluted workspace) was only 0.45 ($\times 10^3$) µg/m^3, continued increasing and reached its maximum 1 h later [4.19 ($\times 10^3$) µg/m^3]. The 4th scenario, accounting for use of FFR for the entire time period while staying in the polluted workspace, was the 'best-case' scenario as in this particular case the total deposited dose was much lower compared to the BC dose.

The mass concentration was sampled with an instrument based on 120° light scatter (i.e., depending on the particle's refraction index), hence, measured optical diameter needed to be converted to aerodynamic diameter to use the data as an input in the ExDoM2 model. The conversion was done under assumptions that optical diameter equals Stokes diameter, and that the particle density and shape factor are those of the sampled aerosol. This is in many cases (such as in this study) difficult to determine and approximate values are used, which in return, along with the conversion from optical to aerodynamic diameter, can result in incorrect estimation of the particle's diameter.

The transport of particles from one region to another and to the GI tract and lymph nodes is performed mechanically by the airway secretions and cilia movement (mucociliary escalator), airway macrophages, and extrinsic means,

Table 4 Cumulative deposited dose and cumulative retention (µg) in extrathoracic and thoracic region, GI tract and blood after 4 h for **a** Cutting II, **b** SMAW II and **c** TIG II welding

Scenario/Process	Cumulative deposited dose		Cumulative retention			
	Extrathoracic	Thoracic	Extrathoracic	Thoracic	GI	Blood
(a) Cutting II						
Stay (No FFR)	13,408	1296	6790	1011	6194	106
Stay (5 min FFR)	12,051	1233	6129	970	5552	98
Leave after 5 min	1414	78	696	54	665	9
Stay (FFR)	8	1	4	1	4	0
(b) SMAW II						
Stay (No FFR)	7540	1942	4238	1725	3176	102
Stay (5 min FFR)	7497	1931	4217	1715	3155	101
Leave after 5 min	114	18	63	15	48	1
Stay (FFR)	5	1	3	1	2	0
© TIG II						
Stay (No FFR)	344	110	189	98	149	6
Stay (5 min FFR)	331	106	182	95	142	6
Leave after 5 min	88	10	50	9	35	1
Stay (FFR)	0	0	0	0	0	0

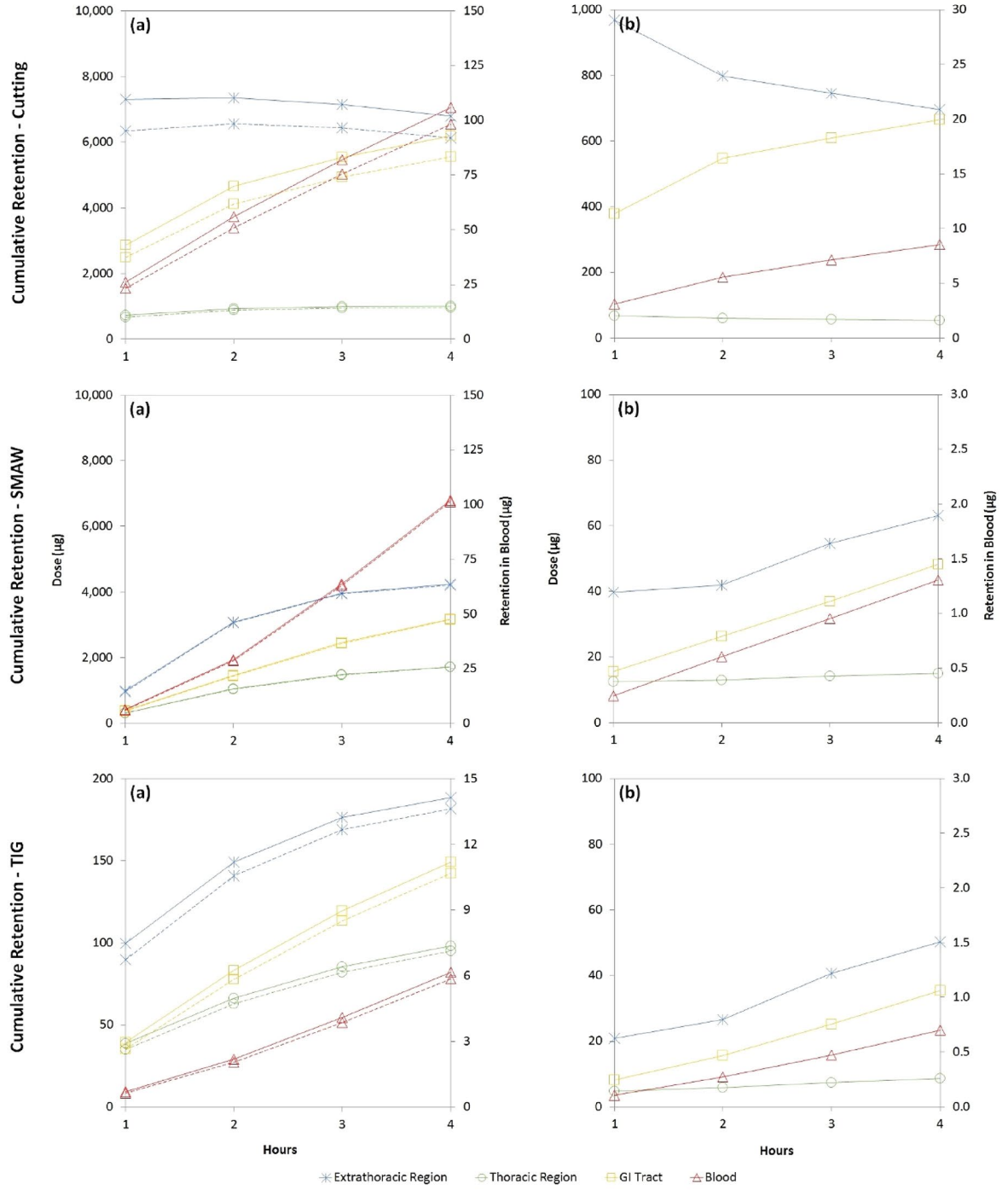

Fig. 4 Cumulative retention (µg) in RT (extrathoracic and thoracic regions), Thoracic region, GI tract, and blood (sec.axis): **a** stay all the time period—No FFR (full line), and Stay all the time period—FFR only during the emission period (dashed line); **b** stay only for the time period of emission (first 5 min)—No FFR and then leave

such as coughing and nose blowing. Particles deposited in the RT are cleared by three main routes: by absorption to the GI tract (via the pharynx), to lymph nodes (via lymphatic channels), and by absorption into blood (depending on the chemical form of deposited particles). As shown in Table 4, the highest dose in all processes was deposited in the extrathoracic region of the RT, where the particles were retained (~53%), entered the oesophagus (GI tract) via pharynx (~44%) or were cleared by nose blowing (~3%). From all 3 processes, deposited dose in extrathoracic region from

cutting (~91%) was higher in every scenario compared to welding processes (~77%). On the contrary, due to higher concentration of fine and ultrafine particles, retained dose in the thoracic region was higher for SMAW and TIG welding processes (~20%) in comparison to cutting (~7%).

The scenarios involving use of FFR in this study were based on FFR filter efficiency only in means of model calculations, i.e., FFR was not challenged with welding fumes, thus pressure drop caused by accumulated welding fumes on the filter (Cho and Yoon 2012) and its effect on FFR's performance was not taken into consideration. Another assumption was that the filtering facepiece fits perfectly and there are no leaks around the face seal. However, penetration levels can increase up to ~50% when the respirator does not have a perfect fit (Serfozo et al. 2017c), which is difficult to achieve especially in the nose-bridge area of the FFR. In addition, most FFRs offer efficient protection against particles larger than ~400 nm, but may be ineffective in providing the expected respiratory protection for workers exposed to nanoparticles (Serfozo et al. 2017a,b). Despite the fact that a poor filtration efficiency and a poor fit may increase under real work conditions, the use of FFR especially in a confined workspace can considerably reduce the exposure to welding fumes.

Particles can be distributed from the blood circulation system to other organs or tissues like liver, kidneys, heart, brain, muscle and bone. Absorption into blood is assumed to occur at the same rate in all regions, except for anterior nasal passage (ET1) where no absorption takes place. As can be seen in Fig. 4a (staying 4 h in the polluted workspace with and without FFR as the most likely scenario in real life), the cumulative retention in the thoracic region was stable after the cutting, while in the case of SMAW and TIG the retention in thoracic region was increasing with time due to higher contribution of respirable particles. Consequently, 16%, 21% and 8% of the total cumulative dose was deposited in the AI region (where the gas exchange takes place) from SMAW, TIG and cutting, respectively. From the particle dose retained in the thoracic region from both welding processes ~6% was absorbed to blood, while in the case of cutting it was ~10%. Nevertheless, the total deposited dose from cutting after the first 1 h (in which the emission occurred) was threefold higher than that from SMAW, after 4 h they had very similar values of blood retention (~100 μg). After 8 h blood retention from SMAW reached 234 μg, while in the case of cutting it was only 180 μg. More importantly, one must consider also the different chemical composition of particles from these two processes deposited and retained in the thoracic region.

In the current study, exposure scenarios with duration of 4 h were examined. However, longer exposure periods to cumulative deposited and retained dose over rather longer time periods of exposure to welding fumes may resulting to adverse health effects (Hannu et al. 2007; Banga et al. 2011; Wittczak et al. 2012; Järvelä et al. 2013; Kauppi et al. 2015).

High concentrations of Mn, especially in a confined workspace, can cause a disease known as 'manganism', characterized by tremor, muscle weakness and rigidity, extreme slowness of movements, or may cause a progression of parkinsonism (Racette et al. 2017). The amount of Mn in welding rods can vary, but most welders are exposed to mixed metal fumes that contain a small percentage of Mn, which was 0.5% in the electrode used in this study, according to the manufacturer. However, latest studies on neurological outcomes associated with low-level Mn exposure suggest that changes can be detected in the brain even at very low levels of exposure among humans before any clinically evident deficits (Baker et al. 2015; Lee et al. 2016), where type and route of exposure play an important role in the extent of Mn-induced toxic effects on the brain (Long et al. 2014). Although the occupational exposure limit (OEL) for Mn vary within the authorities, the American Conference of Governmental Industrial Hygienists (ACGIH) advised threshold limit value (TLV) for Mn to be 20 μg/m^3 for respirable and 100 μg/m^3 for inhalable PM, which however, can be easily exceeded in a confined workspace (Hanley et al. 2015).

On the other hand, metal fumes that contain iron oxide generated at the cutting of SS are considered a nuisance dust with little likelihood of causing chronic lung disease after inhalation. Accumulation of iron oxide in the lungs is called 'siderosis' and is not usually associated with pulmonary fibrosis (lung scarring) and functional impairment of the lungs (Flors Blasco et al. 2010). Abnormalities are reversible and may resolve partially or completely after the worker is removed from the exposure. Moreover, differences between SMAW and TIG welding processes should be addressed with great care as well, even though during TIG significantly less fume is generated, mostly originating from base metal and the external filler metal if used. Brand et al. (2013) monitored the particle size distributions of various welding and joining techniques in standardized laboratory conditions and noted UFP composition differences between processes with high mass emission rates (SMAW) and welding processes with low mass emission rates (TIG). Despite the fact that in all scenarios total dose from TIG in this study had the lowest values, this welding process generates a high number concentration of heavy metal nanoparticles, such as Mn, Cr or Ni (Miettinen et al. 2016) in size range of 15–160 nm (Berlinger et al. 2011).

Although major concerns exist regarding the potential consequences of human exposure to UFP, no human toxicological data is currently available. Study of Andujar et al. (2014) strongly suggest that welding-related UFP could be responsible, at least in part, for the pulmonary inflammation observed in welders. The study by Présumé

et al. (2015, 2016), based upon metal oxide nanoparticles found in lung tissue sections of welders, investigated pulmonary effects in mice of repeated exposure to nanoparticles and demonstrated for the first time a potential risk for respiratory health posed by repeated exposure to nanoparticles at occupationally relevant doses. These results provide, therefore, the first evidence of a link between human exposure to nanoparticles and long-term pulmonary effects. Furthermore, Halatek et al. (2017) confirmed deleterious effect of transitory metals (Cr^{VI}, Mn, Ni) and particles during experimental inhalation exposure to welding dusts, evidenced in the lungs and brain in serum of rats. Their result confirms also the hypothesis about the effect of the welding dusts on the oxidative stress responsible for disturbed systemic homeostasis and impairment of calcium regulation.

4 Conclusions

The current study examined the human deposition and retention dose from SMAW and TIG arc welding processes and cutting of SS in a simulated confined workspace under different scenarios. All 3 investigated processes generated high particle number concentrations ranging from 2.4 to 3.6×10^6 particles/cm^3. Among all 3 processes, PM_{10} concentrations from cutting reached the highest mass emission rates [11 and 22 ($\times 10^3$) μg/m^3], while SMAW had the highest contribution of fine particles [~ 4.1 ($\times 10^3$) μg/m^3], consisting mostly of $PM_{1–2.5}$. The examination of different exposure scenarios revealed that there is only a small difference in respect to deposited dose if the subject would stay in the polluted workspace for the entire investigated time period (4 h) without a use of FFR, or with use of FFR only during the emission period. It would be more beneficial in respect to deposited dose if the exposed subject was not wearing a FFR during the emission but would leave the polluted workspace immediately after the emission period. From all 3 processes, deposited dose in thoracic region from welding processes was higher (~ 23%) in every scenario compared to cutting (~ 9%). When welding occurs in a confined workspace with lower air exchange rate, harmful gases, fumes and nanoparticles may accumulate rapidly and stay airborne for prolonged time periods. As demonstrated in this study, when the total duration of emission was only 1 min for welding processes and 2 min for cutting (in total time period of 5 min per experiment), even a short emission period can cause a great increase of respirable particle concentrations, thus leading to increase in human dose. The approach applied in this study along with toxicological research could be used as an indicator of personal exposure to aerosol of known composition in various workplaces (particularly confined workspaces).

Acknowledgements The author gratefully acknowledges the financial support of the European Commission under Grant HEXACOMM, which was funded from the H2020 RTD Framework Programme of the European Union (Grant agreement no: 315760). The authors would like also to thank Dr. Polychronis Spanoudakis from School of Production Engineering and Management (Technical University of Crete, Greece) for cooperation and for providing the welding technology.

Funding Open access funding provided by HEAL-Link Greece.

Data availability Data can be obtained from the authors on a reasonable request.

Declarations

Conflict of interest The authors declare that they do not have any conflict of interest.

References

Aleksandropoulou V, Lazaridis M (2013) Development and application of a model (ExDoM) for calculating the respiratory tract dose and retention of particles under variable exposure conditions. Air Qual. Atmos Health 6(1):13–26. https://doi.org/10.1007/s11869-010-0126-z

Andujar P, Simon-Deckers A, Galateau-Sallé F, Fayard B, Beaune G, Clin B et al (2014) Role of metal oxide nanoparticles in histopathological changes observed in the lung of welders. Part Fibre Toxicol 11(1):23

Antonini JM (2006) Design, construction and characterization of a novel robotic welding fume generator and inhalation exposure system for laboratory animals. J Occup Environ Hyg 3:194–203

Antonini JM (2014) Health effects associated with welding. In: Hashmi MSJ (ed) Comprehensive materials processing, vol 8. Elsevier, Amsterdam, pp 49–70

Antonini JM, Keane M, Chen BT, Stone S, Roberts JR, Schwegler-Berry D, Andrews RN, Frazer DG, Sriram K (2011) Alterations in welding process voltage affect the generation of ultrafine particles, fume composition, and pulmonary toxicity. Nanotoxicol 5(4):700–710

Avino P, Manigrasso M, Pandolfi P, Tornese C, Settimi D, Paolucci N (2015) Submicron particles during macro- and micro-weldings procedures in industrial indoor environments and health implications for welding operators. Metals 5(2):1045–1060

Baker MG, Criswell SR, Racette BA, Simpson CD, Seixas NS, Checkoway H, Sheppard L (2015) Neurological outcomes associated with low-level manganese exposure in an inception cohort of asymptomatic welding trainees. Scand J Work Environ Health 41(1):94–101

Banga A, Reilly MJ, Rosenman KD (2011) A study of characteristics of Michigan workers with work-related asthma exposed to welding. J Occup Environ Med 53(4):415–419

Baracchini E, Bianco C, Crosera M, Filon FL, Belluso E, Caprlla S, Maina G, Adami G (2018) Nano- and submicron particles emission during gas tungsten arc welding (GTAW) of steel: differences between automatic and manual process. Aerosol Air Qual Res 18(3):579–589

Berlinger B, Benker N, Weinbruch S, L'Vov B, Ebert M, Koch W, Ellingsen DG, Thomassen Y (2011) Physicochemical characterisation of different welding aerosols. Anal Bioanal Chem 399(5):1773–1780

Bowler RM, Nakagawa S, Drezgic M, Roels HA, Park RM, Diamond E et al (2007) Sequelae of fume exposure in confined space welding: a neurological and neuropsychological case series. Neurotoxicology 28(2):298–311

Brand P, Lenz K, Reisgen U, Kraus T (2013) Number size distribution of fine and ultrafine fume particles from various welding processes. Ann Occup Hyg 57(3):305–313

Chalvatzaki E, Lazaridis M (2015) Development and application of a dosimetry model (ExDoM2) for calculating internal dose of specific particle-bound metals in the human body. Inhal Toxicol 27(6):308–320

Chalvatzaki E, Chatoutsidou SE, Martins V, Faria T, Diapouli E, Manousakas M, Almeida SM, Eleftheriadis K, Lazaridis M (2020) Assessment of the personal dose received by school children due to pm10 air pollution in Lisbon. Aerosol Air Qual Res 20:1384–1397

Chalvatzaki E, Chatoutsidou SE, Lazaridis M (2022) Regional deposited dose in the human respiratory tract using different particulate metrics. J Environ Expo Assess 1:18

Cho H-W, Yoon C-S (2012) Workplace field testing of the pressure drop of particulate respirators using welding fumes. Ann Occup Hyg 56(8):948–958

Debia M, Weichenthal S, Dufresne A (2014) Case study: ultrafine particles exposure in apprentice welders. J Occup Environ Hyg 11(2):D1–D9

Ennan AA, Kiro SA, Oprya MV, Vishnyakov VI (2013) Particle size distribution of welding fume and its dependency on conditions of shielded metal arc welding. J Aero Sci 64:103–110

Flors Blasco L, Domingo ML, Leiva-Salinas C, Mazón M, Roselló-Sastre E, Vilar J (2010) Uncommon occupational lung diseases: high-resolution CT findings. Am J Roentgenol 194(1):W20–W26

Flynn MR, Susi P (2012) Local exhaust ventilation for the control of welding fumes in the construction industry—a literature review. Ann Occup Hyg 56(7):764–776

Graczyk H, Lewinski N, Zhao J, Concha-Lozano N, Riediker M (2015) Characterization of tungsten inert gas (TIG) welding fume generated by apprentice welders. Ann Occup Hyg 60(2):205–219

Guerreiro C, Gomes JF, Carvalho P, Santos TJG, Miranda RM, Albuquerque P (2014) Characterization of airborne particles generated from metal active gas welding process. Inhal Toxicol 26(6):345–352

Halatek T, Stanislawska M, Kaminska I, Cieslak M, Swiercz R, Wasowicz W (2017) The time-dependent health and biochemical effects in rats exposed to SS welding dust and its soluble form. J Environ Sci Health A Tox Hazard Subst Environ Eng 52(3):265–273

Hanley KW, Andrews R, Bertke S, Ashley K (2015) Manganese fractionation using a sequential extraction method to evaluate welders shielded metal arc welding exposures during construction projects in oil refineries. J Occup Environ Hyg 12(11):774–784

Hannu T, Piipari R, Tuppurainen M, Nordman H, Tuomi T (2007) Occupational asthma caused by stainless steel welding fumes: a clinical study. Eur Respir J 29(1):85–90

Hariri A, Leman AM, Yusof MZM (2013) Experimental study on welding fumes exposure from aluminum metal inert gas (MIG) process. Adv Mat Res 701:382–386

Hinds WC (1999) Aerosol technology: properties, behavior, and measurement of airborne particles. John Wiley & Sons, New York (**ISBN: 978-0-471-19410-1**)

Hobson A, Seixas N, Sterling D, Racette BA (2011) Estimation of particulate mass and manganese exposure levels among welders. Ann Occup Hyg 55(1):113–125

ICRP (2015) ICRP Publication 130: Occupational Intakes of Radionuclides: Part 1. Ann ICRP 44(2). https://doi.org/10.1177/0146645315577539

Järvelä M, Kauppi P, Tuomi T, Luukkonen R, Lindholm H, Nieminen R, Moilanen E, Hannu T (2013) Inflammatory response to acute exposure to welding fumes during the working day. Int J Occup Med Environ Health 26(2):220–229

Kauppi P, Järvelä M, Tuomi T, Luukkonen R, Lindholm T, Nieminen R, Moilanen E, Hannu T (2015) Systemic inflammatory responses following welding inhalation challenge test. Toxicol Rep 2:357–364

Lee E-Y, Flynn MR, Du G, Lewis MM, Herring AH, Van Buren E et al (2016) Lower fractional anisotropy in the globus pallidus of asymptomatic welders, a marker for long-term welding exposure. Toxicol Sci 153(1):165–173

Lehnert M, Pesch B, Lotz A, Pelzer J, Kendzia B, Gawrych K et al (2012) Exposure to inhalable, respirable, and ultrafine particles in welding fume. Ann Occup Hyg 56(5):557–567

Lin C-C, Chen M-R, Chang S-L, Liao W-H, Chen H-L (2015) Characterization of ambient particles size in workplace of manufacturing physical fitness equipments. Ind Health 53:78–84

Long Z, Jiang Y-M, Li X-R, Fadel W, Xu J, Yeh CL et al (2014) Vulnerability of welders to manganese exposure—a neuroimaging study. Neurotoxicology 45(1):285–292

Miettinen M, Torvela T, Leskinen JTT (2016) Physicochemical characterization of aerosol generated in the gas tungsten arc welding of stainless steel. Ann Occup Hyg 60(8):960–968

Oprya M, Kiro S, Worobiec A, Horemans B, Darchuk L, Novakovic V, Ennan A, Van Grieken R (2012) Size distribution and chemical properties of welding fumes of inhalable particles. J Aero Sci 45:50–57

Paridokht F, Soury S, Zeverdegani SK (2023) The simulation of the emission of iron fumes caused by shielded metal arc welding using a computational fluid dynamics method. Toxicol Ind Health 39:36–48

Pouzou JG, Warner C, Neitzel RL, Croteau GA, Yost MG, Seixas NS (2015) Confined space ventilation by shipyard welders: observed use and effectiveness. Ann Occup Hyg 59(1):116–121

Présumé M, Attoui M, Maisser A, Petit G, Lanone S (2015) Design and characterization of an inhalation system of iron and manganese oxide nanoparticles for rodent exposure. Aerosol Sci Tech 49(8):580–588

Présumé M, Simon-Deckers A, Tomkiewicz-Raulet C, Le Grand B, Tran Van Nhieu J, Beaune G et al (2016) Exposure to metal oxide nanoparticles administered at occupationally relevant doses induces pulmonary effects in mice. Nanotoxicology 10(10):1535–1544

Quémerais B, Mino J, Amin MR, Golshahi H, Izadi H (2015) Detailed characterization of welding fumes in personal exposure samples. J Phys Conf Ser 617(1):012011

Racette BA, Nielsen SS, Criswell SR, Sheppard L, Seixas N, Warden MN, Checkoway H (2017) Dose-dependent progression of parkinsonism in manganese-exposed welders. Neurology 88(4):344–351

Serfozo, N. (2017). Estimation of emission rates and lung dose from various simulated indoor workplace related aerosol species. PhD Thesis. School of Chemical and Environmental Engineering, Technical University of Crete

Serfozo N, Ondráček J, Zíková N, Lazaridis M, Ždímal V (2017a) Size-resolved penetrations of filtering materials from CE-marked filtering facepiece respirators. Aerosol Air Qual Res 17(5):1305–1315

Serfozo N, Ondráček J, Otáhal P, Lazaridis M, Ždímal V (2017b) Manikin-based size-resolved penetrations of ce-marked filtering facepiece respirators. J Occup Environ Hyg 14(12):965–974

Serfozo N, Glytsos T, Ondráček J, Lazaridis M (2018) Evaluation of nanoparticle emissions from a laser printer in an experimental chamber and estimation of the human particle dose. Environ Sci Pollut Res 25:13103–13117

Smolík J, Lazaridis M, Moravec P, Schwarz J, Zaripov SK, Ždímal V (2005) Indoor aerosol particle deposition in an empty office. Water Air Soil Poll 165:301–312

Su WC, Chen Y, Bezerra M, Wang J (2019) Respiratory deposition of welding fume particles. J Occup Environ Hyg 16:694–706

Tian L, Inthavong K, Lidé G, Shang Y, Tu J (2016) Transport and deposition of welding fume agglomerates in a realistic human nasal airway. Ann Occup Hyg 60(6):731–747

Vishnyakov VI, Kiro SA, Oprya MV, Ennan AA (2014a) Coagulation of charged particles in self-organizing thermal plasmas of welding fumes. J Aero Sci 76:138–147

Vishnyakov VI, Kiro SA, Ennan AA (2014b) Multicomponent condensation in the plasma of welding fumes. J Aero Sci 74:1–10

Vishnyakov VI, Kozytskyi SV, Ennan AA (2019) Features of nucleation in welding fumes from gas metal arc welding. J Aerosol Sci. https://doi.org/10.1016/j.jaerosci.2019.105439

Ward RX, Tilly TB, Mazhar SI, Robinson SE, Eiguren-Fernandez A, Wang J, Sabo-Attwood T, Wu CY (2020) Mimicking the human respiratory system: online in vitro cell exposure for toxicity assessment of welding fume aerosol. J Hazard Mater 395:122687

Wittczak T, Dudek W, Walusiak-Skorupa J, Swierczynska-Machura D, Cader W, Kowalczyk M, Palczynski C (2012) Metal-induced asthma and chest X-ray changes in welders. Int J Occup Med Environ Health 25(3):242–250